

**Supplementary Materials for**  
**Discovery of Main Group Single Sb-N<sub>4</sub> Active Sites for CO<sub>2</sub>**  
**Electroreduction to Formate with High Efficiency**

Zhuoli Jiang,<sup>‡ a</sup> Tao Wang,<sup>‡ b</sup> Jiajing Pei,<sup>‡ c</sup> Huishan Shang,<sup>a</sup> Danni Zhou,<sup>a</sup> Haijing Li,<sup>d</sup>  
Juncai Dong,<sup>d</sup> Yu Wang,<sup>e</sup> Rui Cao,<sup>f</sup> Zhongbin Zhuang,<sup>c</sup> Wenxing Chen,<sup>\*a</sup> Dingsheng  
Wang,<sup>\*g</sup> Jiatao Zhang,<sup>\*a</sup> and Yadong Li<sup>g</sup>

<sup>a</sup> Beijing Key Laboratory of Construction Tailorable Advanced Functional Materials and Green Applications, School of Materials Science and Engineering, Beijing Institute of Technology, Beijing 100081, China

<sup>b</sup> SUNCAT Center for Interface Science and Catalysis, Department of Chemical Engineering, Stanford University, Stanford, California 94305, USA

<sup>c</sup> College of Chemical Engineering, Beijing University of Chemical Technology, Beijing 100029, China

<sup>d</sup> Beijing Synchrotron Radiation Facility, Institute of High Energy Physics, Chinese Academy of Sciences, Beijing, China

<sup>e</sup> Shanghai Synchrotron Radiation Facility, Shanghai Institute of Applied Physics, Chinese Academy of Science, Shanghai 201800, China

<sup>f</sup> Stanford Synchrotron Radiation Lightsource, SLAC National Accelerator Laboratory, Menlo Park, CA, 94025, USA

<sup>g</sup> Department of Chemistry, Tsinghua University, Beijing 100084, China

‡ These authors contributed equally to this work.

\* Corresponding author. E-mail: wxchen@bit.edu.cn, zhangjt@bit.edu.cn, wangdingsheng@mail.tsinghua.edu.cn.

## **Table of contents**

- 1. Experiment detail**
- 2. Supplementary Figures and Tables**
- 3. References**

## 1. Experiment detail

**Reagents.** Antimony Trichloride ( $\text{SbCl}_3$ ), Indium Trichloride ( $\text{InCl}_3$ ), Tin chloride ( $\text{SnCl}_4$ ), Bismuth chloride ( $\text{BiCl}_3$ ), dicyandiamide (DCDA), Trimesic acid and Nafion D-521 dispersion (5% w/w in water and 1-propanol) were purchased from Alfa Aesar. Ethanol and  $\text{KHCO}_3$  were obtained from Sinopharm Chemical. Sulphuric acid ( $\text{H}_2\text{SO}_4$ ) (98%) was obtained from Beijing Chemical Reagents. The deionized water used in all experiments was obtained through ion-exchange and filtration. All the chemicals were analytical grade and used without further purification.

### Preparation of Sb SAs/NC

In a typical procedure of Sb SAs/NC catalyst, 50 mg antimonous chloride ( $\text{SbCl}_3$ ), 1.0 g dicyandiamide (DCDA) and 0.1g trimesic acid were dissolved in 5 mL of ethanol under ultrasound for 5 min at room temperature. Then, the mix solution was continuously stirred and dried at 80 °C. The obtained dried mixture was placed in the porcelain boat. The porcelain boat was placed in a quartz tube of a horizontal furnace. And then, the boat was annealed at 800 °C under the  $\text{N}_2$  atmosphere for 2 h with a ramping rate of 5 °C/min, then cooled down to room temperature. Subsequently, the samples were leached in 0.5 M  $\text{H}_2\text{SO}_4$  solution at 80 °C for 24 h to remove the metallic Sb nanoparticles, and washed thoroughly with ethanol and deionized water. Finally, the samples were dried in vacuum at 60 °C for overnight.

### Preparation of Sb NPs/C

50 mg  $\text{SbCl}_3$  and 0.1g trimesic acid were dissolved in 5 mL of deionized water under vigorous stirring. Then, the mix solution was continuously stirred and dried at 80 °C. The obtained dried mixture was placed in the porcelain boat. The porcelain boat was placed in a quartz tube of a horizontal furnace. And then, the boat was annealed at 800 °C under the  $\text{N}_2$  atmosphere for 2 h with a ramping rate of 5 °C/min, then cooled down to room temperature.

### Preparation of NC

Trimesic acid (0.1 g) and DCDA (1.0 g) were mixed by grinding and annealed from room temperature to 800 °C with a heating rate of 5 °C /min under a  $\text{N}_2$  flow. After calcining for further 2 h at the desired temperature, the sample was naturally cooled to room temperature, denoted as NC.

### **Preparation of In SAs/NC, Sn SAs/NC and Bi SAs/NC**

Same method as synthesizing Sb SAs/NC, except replacing the precursor  $\text{SbCl}_3$  with 50 mg  $\text{InCl}_3$ ,  $\text{SnCl}_4$  and  $\text{BiCl}_3$ , respectively.

**Characterizations.** The morphology of the samples was characterized by transmission electron microscope (TEM, FEI Tecnai G2 20) with an accelerating voltage of 200 kV. The HAADF-STEM images were obtained by JEOL JEM-ARM200F at an accelerating voltage of 200 kV. The crystal phases present in each sample were identified using powder X-ray diffraction (XRD) patterns were recorded on a Y-2000 X-ray Diffractometer with copper  $\text{K}\alpha$  radiation ( $\lambda=1.5406 \text{ \AA}$ ) at 40 kV, 40 mA. The Raman measurements were taken on a Renishaw spectrometer at 532 nm on a Renishaw Microscope System RM2000. The  $\text{N}_2$  adsorption/desorption curve was carried out by BET measurements using a Micromeritics ASAP 2020 surface area analyzer.

**Electrochemical measurements for  $\text{CO}_2\text{RR}$ .** 2mg of the catalyst and 10  $\mu\text{l}$  Nafion solution (5wt%) ultrasonically dispersed in the mixture of deionized water/ethanol (volume ratio, 1 : 4) for at least 30 min to yield a well-dispersed catalyst ink with a concentration of 2  $\text{mg mL}^{-1}$ . Electrochemical measurements were carried out on CHI 760E electrochemical workstation (Shanghai Chenhua, China) with a gas-tight H-type cell in 50 ml 0.5 M  $\text{KHCO}_3$  electrolyte. Nafion 117 membrane was inserted between the cathodic chamber and anodic chamber. A Pt plate and an Ag/AgCl (saturated KCl) electrode were used as the counter electrode and reference electrode, respectively. Electrode potentials conversion formula:  $E_{\text{RHE}} = E_{\text{Ag/AgCl}} + 0.197 \text{ V} + 0.0591 \times \text{pH}$ . The electrolyte was 0.5 M  $\text{KHCO}_3$ . 10  $\mu\text{L}$  of the catalyst ink prepared above was dropped on a glassy carbon (GC) electrode with a surface area of 0.196  $\text{cm}^2$  and the catalyst loading was 0.102  $\text{mg cm}^{-2}$ . Before all measurements,  $\text{CO}_2$  flow were used through the electrolyte in the cell for 30 min to obtain  $\text{CO}_2$ -saturated electrolyte. The cyclic voltammetry (CV) experiments were cycled in  $\text{CO}_2$ -saturated 0.5 M  $\text{KHCO}_3$  with a scan rate of 50  $\text{mV s}^{-1}$ , and the linear sweep voltammetry (LSV) experiments were cycled in  $\text{CO}_2$ -saturated 0.5 M  $\text{KHCO}_3$  with a scan rate of 10  $\text{mV s}^{-1}$ . All the potential was reported versus the reversible hydrogen electrode (RHE).

**Flow cell measurements.** An organic glass cell was employed for the flow cell experiments. We deposited Sb SAs/NC on a gas diffusion layer as the working electrode.

Electrolyte is CO<sub>2</sub>-saturated 1 M KHCO<sub>3</sub> and 1 M KOH solution, respectively. During the test, maintain the continuous CO<sub>2</sub> flow and electrolyte flow.

### **CO<sub>2</sub>RR products analysis**

CO<sub>2</sub> reduction products were measured by gas chromatography (GC, Shimadzu 2010) and nuclear magnetic resonance (NMR, Bruker 400 MHz) for the gas and liquid products, respectively. Both instruments were calibrated with standard gases or liquid solutions. For real-time gas phase product analysis, the outlet of the cathode compartment was connected to the GC inlet. As reported previously, the GC system used an automatic valve injection (1 mL sample) and a thermal conductivity detector (TCD) and flame ionization detector (FID). Ultra-high purity nitrogen (99.99%, Specialty Gases) was used as the carrier gas for all experiments and was chosen to enable accurate hydrogen quantification. In addition, NMR spectroscopy was used to analyze and quantify the products in the liquid phase by performing <sup>1</sup>H NMR experiments. Samples were prepared by mixing DMSO and electrolyte aliquots in a 1:1 volume ratio. Faradaic efficiency (F.E.) was calculated for the chronoamperometric measurements by determining the charge required to produce the measured product concentration and dividing by the total charge passed during the time the sample underwent electrolysis.

#### ***Gaseous Products:***

$$FE_{gas}(\%) = \frac{Q_{gas}}{Q_{total}} \times 100\% = \frac{\left(\frac{v}{60s/min}\right) \times \left(\frac{V_{gas}}{22400cm^3/mol}\right) \times N \times F \times 100\%}{j}$$

$v$  is gas flow rate measured by a flowmeter at the exit of the cell at room temperature.

$V_{gas}$  is volume concentration of CO or H<sub>2</sub> in the exhaust gas from the cell.

$N = 2$  is the number of electrons required to form a molecule of CO or H<sub>2</sub>.

$F$  is the Faraday constant (96485 C mol<sup>-1</sup>).

$j$  is the recorded current.

#### ***Liquid Products:***

$$FE_{HCOO^-}(\%) = \frac{Q_{HCOO^-}}{Q_{total}} \times 100\% = \frac{n_{HCOO^-} \times N \times F \times 100\%}{j \times t}$$

$n_{HCOO^-}$  is the measured amount of formate in the cathodic compartment.

$t$  is the reaction time.

$$j_{\text{HCOO}^-}(\%) = FE_{\text{HCOO}^-}(\%) \times j$$

$j_{\text{HCOO}^-}$  is  $\text{HCOO}^-$  partial current density.

**XPS and Soft-XAS measurements.** XPS experiments were performed at the Photoemission Endstation at the BL10B beamline in the National Synchrotron Radiation Laboratory (NSRL) in Hefei, China. The XANES spectra (C K-edge and N K-edge) were performed at beamline BL12B of National Synchrotron Radiation Laboratory (NSRL) in Hefei, China. The samples were deposited onto double-sided carbon tape for X-ray spectroscopy. A bending magnet was connected to the beamline BL12B, which was equipped with three gratings covering photon energies from 100 to 1,000 eV with an energy resolution of  $\sim 0.2$  eV. The data were recorded in the total electron yield mode by collecting the sample drain current. The resolving power of the grating was typically  $E/\Delta E = 1,000$ , and the photon flux was  $1 \times 10^{10}$  photons per second.

**Ex-situ XAFS measurements.** The XAFS spectra data (Sb K-edge, In K-edge, Sn K-edge and Bi  $L_3$ -edge) were tested at 14W1 station in Shanghai Synchrotron Radiation Facility (SSRF, operated at 3.5 GeV with a maximum current of 250 mA). The XAFS data of the samples were collected at room temperature in fluorescence excitation mode using a Lytle detector. All the samples were added with graphite and ground uniformly, and then pressed into a 10 mm plate with a thickness of 1 mm.

### **XAFS data processing**

The received EXAFS data were processed according to the standard procedures using the Athena and Artemis implemented in the IFEFFIT software packages. The fitting detail is depicted in the following:

The EXAFS spectra were obtained by subtracting the post-edge background from the overall absorption and then normalizing relative to the edge-jump step. Subsequently, the  $\chi(k)$  data were Fourier transformed to real (R) space using a hanning windows ( $dk=1.0 \text{ \AA}^{-1}$ ) to separate the EXAFS contributions from different coordination shells. To obtain the quantitative structural parameters around central atoms, least-squares curve parameter fitting was performed using the ARTEMIS module of IFEFFIT software packages.<sup>11</sup>

The following EXAFS equation was used:

$$\chi(k) = \sum_j \frac{N_j S_o^2 F_j(k)}{k R_j^2} \exp[-2 k^2 \sigma_j^2] \exp\left[-\frac{2 R_j}{\lambda(k)}\right] \sin[2k R_j + \phi_j(k)]$$

$S_o^2$  is the amplitude reduction factor,  $F_j(k)$  is the effective curved-wave backscattering amplitude,  $N_j$  is the number of neighbors in the  $j^{\text{th}}$  atomic shell,  $R_j$  is the distance between the X-ray absorbing central atom and the atoms in the  $j^{\text{th}}$  atomic shell (backscatterer),  $\lambda$  is the mean free path in Å,  $\phi_j(k)$  is the phase shift (including the phase shift for each shell and the total central atom phase shift),  $\sigma_j$  is the Debye-Waller parameter of the  $j^{\text{th}}$  atomic shell (variation of distances around the average  $R_j$ ). The functions  $F_j(k)$ ,  $\lambda$  and  $\phi_j(k)$  were calculated with the ab initio code FEFF8.2.<sup>12</sup> The additional details for EXAFS simulations are given below.

The coordination numbers of model samples (Sb foil) were fixed as the nominal values. The obtained  $S_o^2$  was fixed in the subsequent fitting of Sb single atom samples. While the internal atomic distances  $R$ , Debye-Waller factor  $\sigma^2$ , and the edge-energy shift  $\Delta E_0$  were allowed to run freely.

***In-situ* XAFS measurements.** Electrochemical measurements were conducted on a computer-controlled electrochemical analyzer. A catalyst modified carbon paper was used as working electrode, Pt plate as counter electrode and Ag/AgCl (KCl-saturated) electrode as reference electrode. An organic glass electrochemical cell was employed for the in-situ experiments. The working cell has flat walls with a single circular hole of 1.5 cm in diameter. Sb SAs/NC coated carbon paper was in contact with a slip of copper with the Sb SAs/NC layer facing inward. Then  $\text{KHCO}_3$  solution was poured into the cell. The solutions were not stirred during the experiment. The cell was connected to an electrochemical station by making electrical contact to the copper tape slip that protruded from the side of the working cell. An organic glass cap fitted with a reference electrode (Ag/AgCl) was used to cover the cell and to ensure a fixed distance between working and reference electrodes for all experiments. The XAFS spectra were recorded at different positions on the electrode to check the homogeneity of the catalyst.

**Computational details.** All the DFT simulations were carried out with the Vienna Ab Initio Simulation Package (VASP),<sup>1,2</sup> and the electron ion interaction was described with the projector augmented wave (PAW) method.<sup>3,4</sup> The electron exchange and correlation

energy was solved with the revised Perdew-Burke-Ernzerhof (RPBE) exchange-correlation functional within the generalized gradient approximation.<sup>5</sup> The energy cut-off was set to be 400 eV, and a second-order Methfessel-Paxton electron smearing with  $\sigma = 0.2$  eV was utilized to guarantee the accuracy. The convergences criteria for energy and force are set to be  $10^{-5}$  eV and  $0.02$  eV/Å, respectively. A vacuum layer of  $15$  Å was set between the periodically repeating slabs. Spin polarization was included throughout all the calculations.

The Sb SAs/NC catalyst was modeled by a  $p(4\times 4)$  supercell of graphene doped with nitrogen and Sb atoms, where Sb coordinated with four neighboring N atoms as shown in Fig. S25. As comparisons, the Sb NPs/C catalyst was modeled a  $p(3\times 3)$ -Sb(111) surface supercell as given in Fig. S26 and a  $p(4\times 4)$  supercell of graphene doped with only nitrogen was used to model the NC catalyst as shown in Fig. S27. The  $(3\times 3\times 1)$  Monkhorst–Pack grid K-points was used to sample the Brillouin zone for all models. The most stable adsorption configurations of  $\text{HCOO}^*$ ,  $\text{COOH}^*$ ,  $\text{CO}^*$  and  $\text{H}^*$  species on the Sb SAs/NC, Sb NPs/C and NC were given in Figs. S25-S27. The free energies of all the reaction mechanisms in this work were calculated with computational hydrogen electrode (CHE) model as developed by Norskov group.<sup>6,7</sup>

## 2. Supplementary Figures and Tables

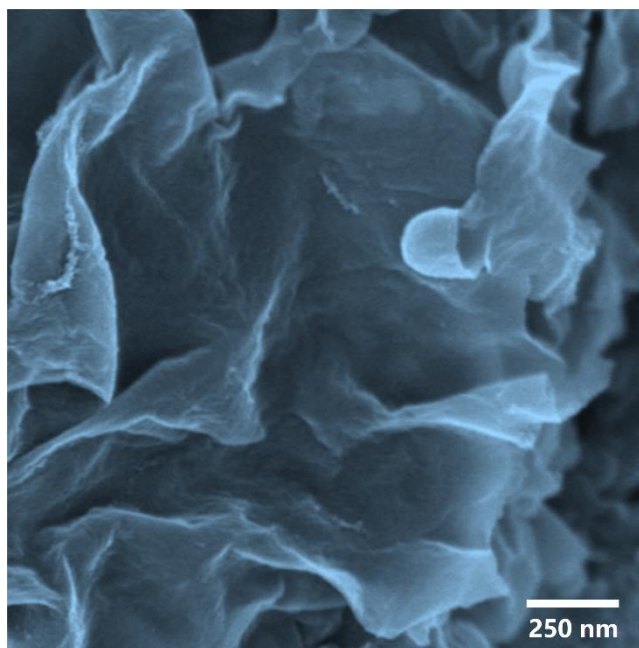


**Fig. S1.** SEM image of the Sb SAs/NC.

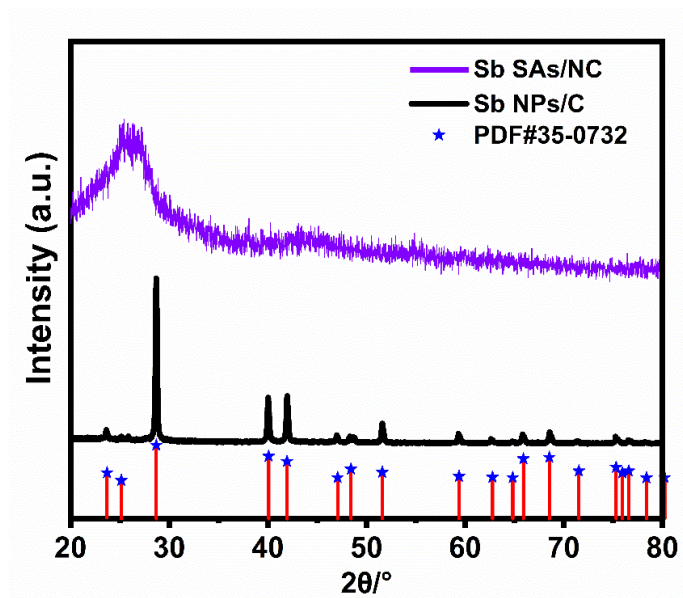


**Fig. S2.** XRD patterns of Sb NPs/C and Sb SAs/NC. PDF#35-0732 corresponds to metallic Sb.

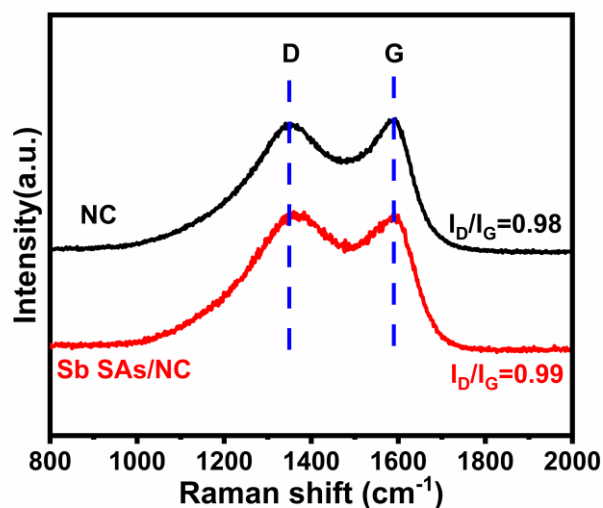


**Fig. S3.** Raman spectra of the Sb SAs/NC and NC samples. There are only two characteristic peaks of carbon including D band (disordered/defective carbon) and G band (graphitic carbon) in the Raman spectra. The high ratio  $I_D/I_G$  of Sb SAs/NC means that plenty of defects may exist in the carbon matrix.<sup>8</sup>

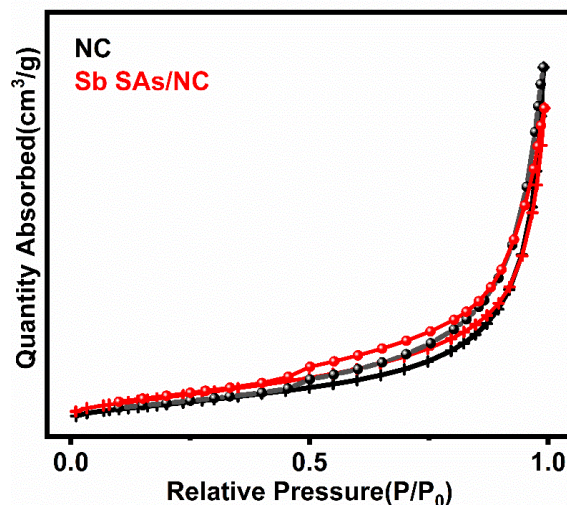


**Fig. S4.** Brunauer–Emmett–Teller (BET) analysis.  $N_2$  adsorption-desorption isotherms of Sb SAs/NC and NC. Surface area of the catalyst sample was calculated by using the BET method. The BET specific higher surface area measured for Sb SAs/NC was  $339.4 \text{ m}^2 \text{ g}^{-1}$  than that of NC ( $297.6 \text{ m}^2 \text{ g}^{-1}$ ).

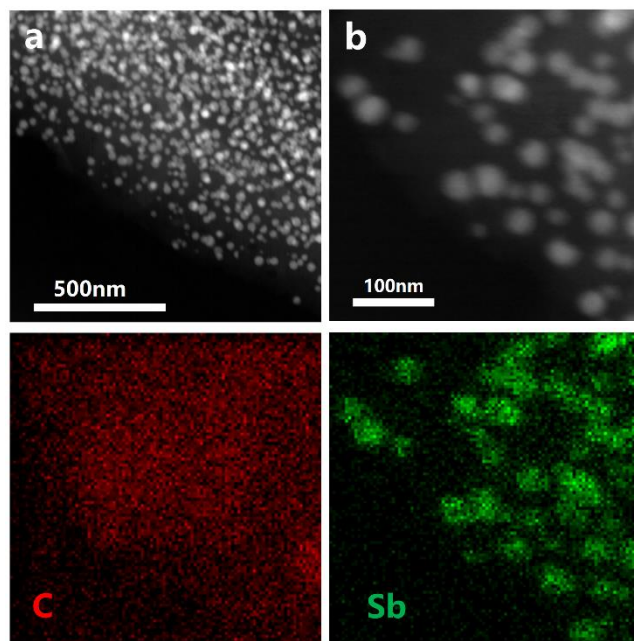


**Fig. S5.** TEM and EDS images of Sb NPs/C.

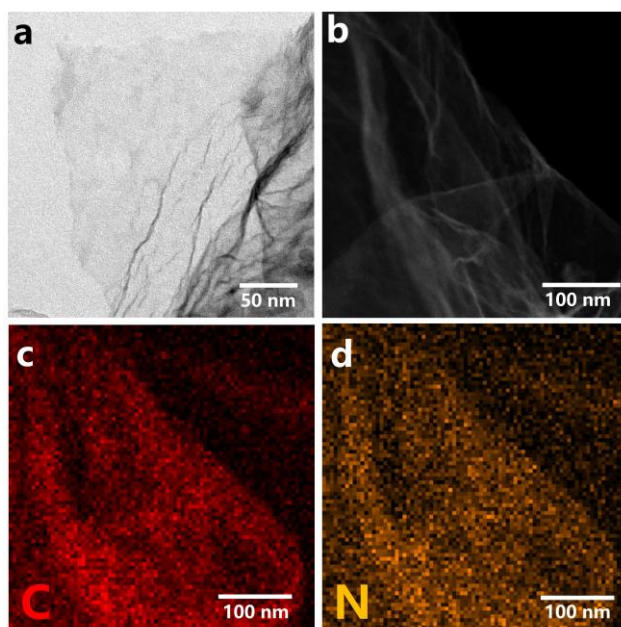


**Fig. S6.** TEM and EDS images of N-doped carbon sheets (NC).

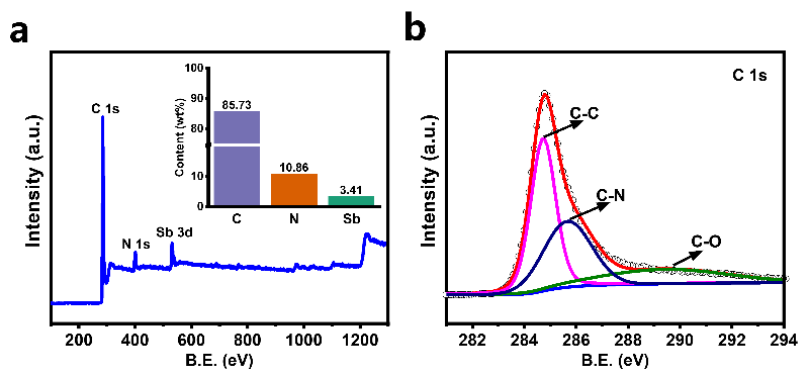


**Fig. S7.** XPS spectra of Sb SAs/NC. (a) XPS survey (inset image is the weight content percentages of C, N and Sb in Sb SAs/NC measured by XPS analysis). (b) C 1s spectrum.

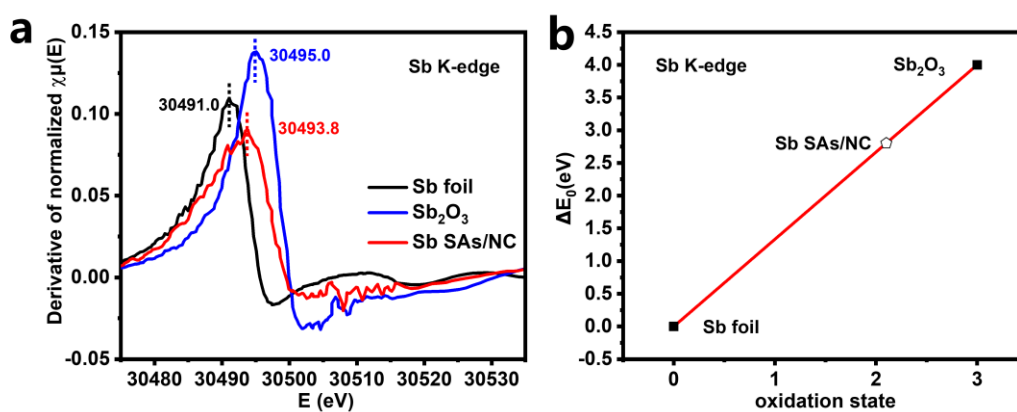


**Fig. S8.** (a) First-derivative XANES curves of Sb SAs/NC and the references at Sb K-edge. (b) The average oxidation state of Sb in Sb SAs/NC from XANES spectra.

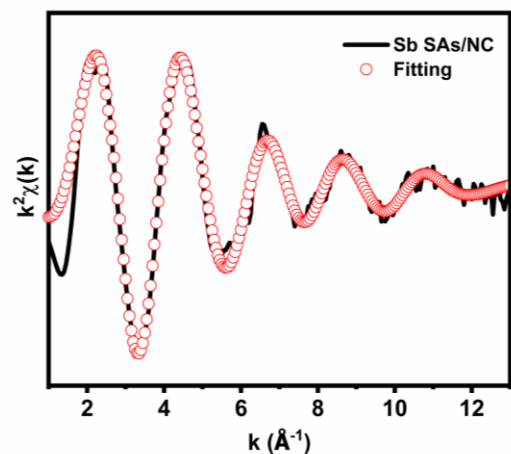


**Fig. S9.** EXAFS  $k$  space fitting curve (circle) and the experimental one (line) of Sb SAs/NC.

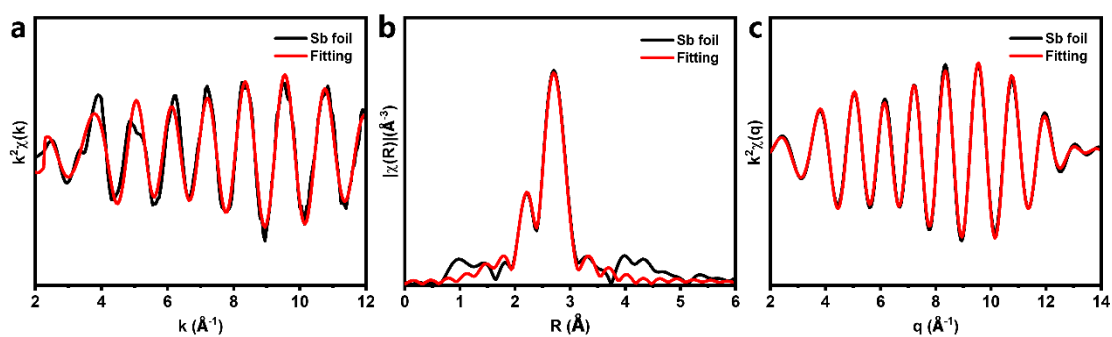


**Fig. S10.** (a)  $k$  space EXAFS, (b) FT-EXAFS and (c) inverted FT-EXAFS fitting curves of Sb foil.

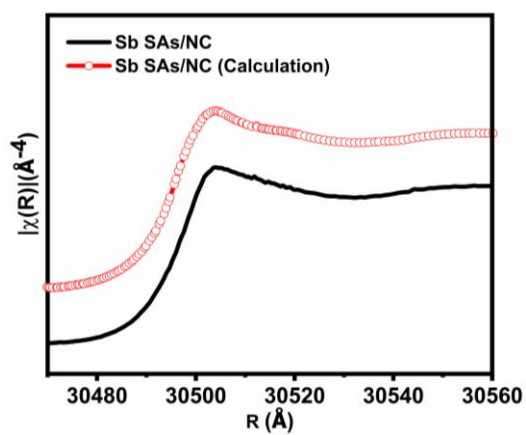


**Fig. S11.** Experimental XANES and calculated XANES curves of Sb SAs/NC at Sb K-edge.

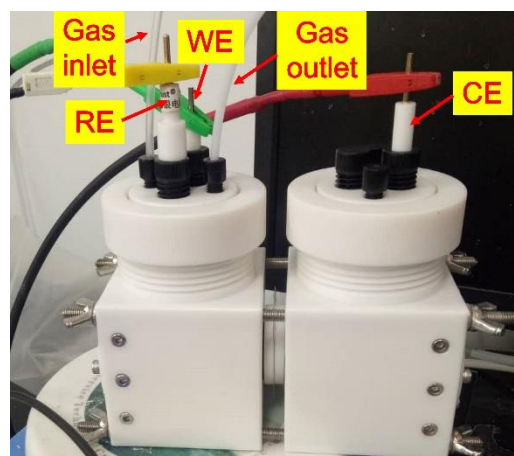


**Fig. S12.** Gas-tight H-type cell for the electrochemical CO<sub>2</sub>RR measurements.

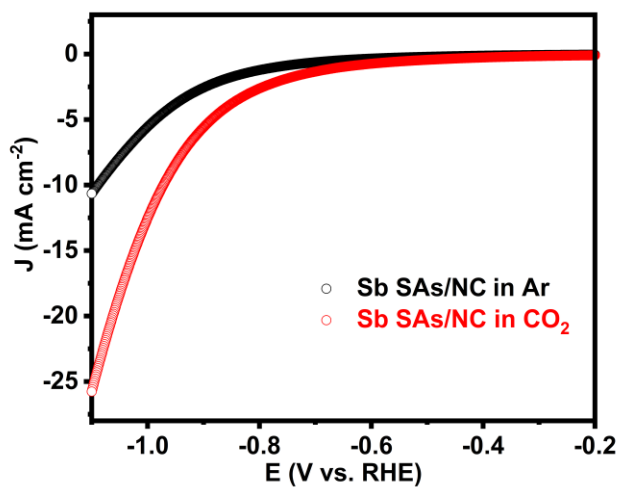


**Fig. S13.** LSV curves of Sb SAs/NC in Ar- and CO<sub>2</sub>- saturated 0.5M KHCO<sub>3</sub> at the scan rate of 10 mV s<sup>-1</sup>.

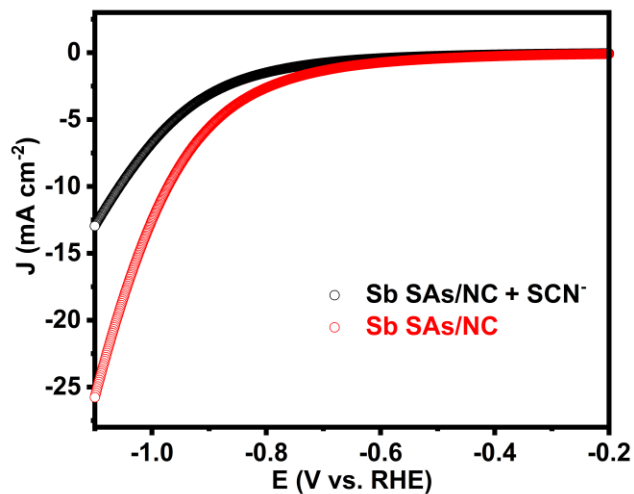


**Fig. S14.** LSV curve of Sb SAs/NC measured in CO<sub>2</sub>-saturated 0.5M KHCO<sub>3</sub> + 0.01 M KSCN solution.

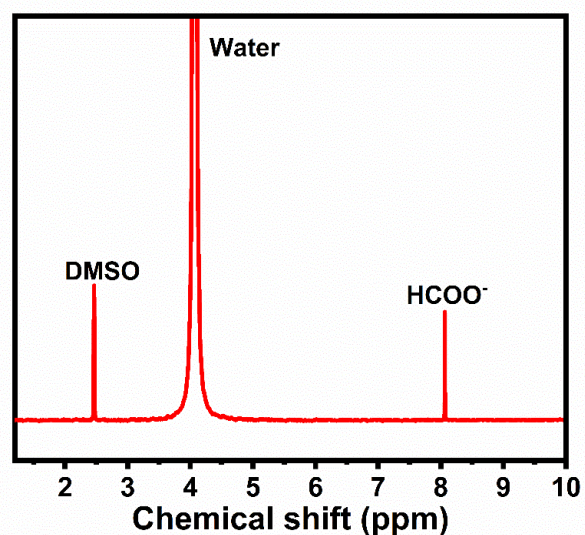


**Fig. S15.** Representative NMR spectrum of the electrolyte after CO<sub>2</sub> reduction electrolysis at -0.8 V vs. RHE for the Sb SAs/NC. NMR experiments were performed using a Varian 400 MHz NMR spectrometer. DMSO is used as an internal standard for quantification of formate.

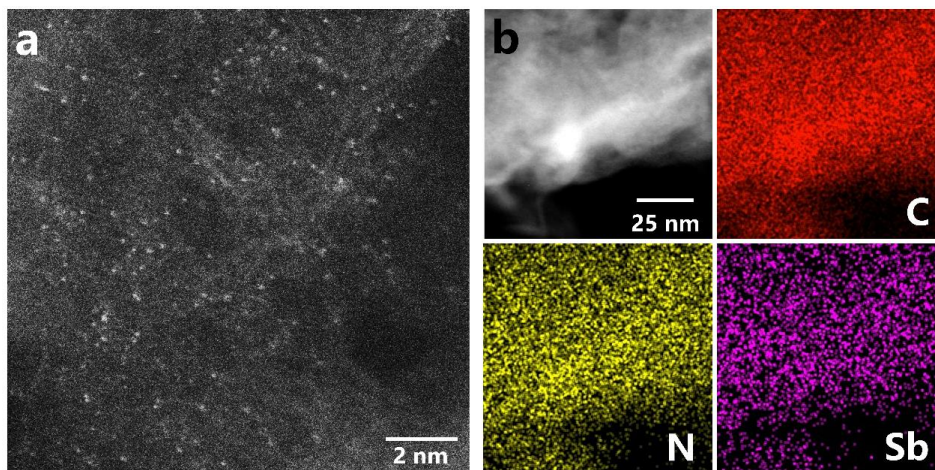


**Fig. S16.** (a) HAADF-STEM image and (b) EDS elemental mapping, with C (red), N (yellow), and Sb (purple) after CO<sub>2</sub> reduction electrolysis for the Sb SAs/NC. Moreover, ICP-OES analysis was performed on the catholyte after electrolysis, and it was found that no Sb species was detected, which demonstrated that no leaching occurred.

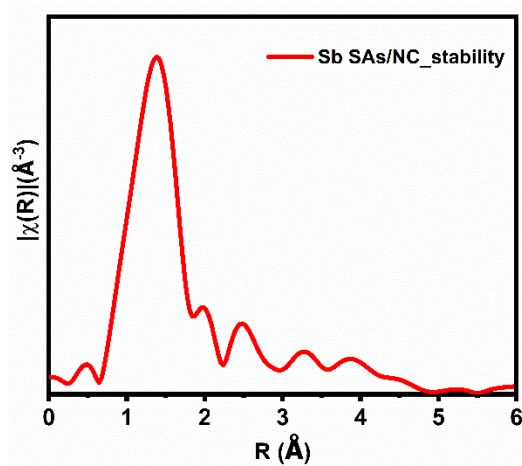


**Fig. S17.** FT-EXAFS spectra of Sb SAs/NC after CO<sub>2</sub> reduction electrolysis.

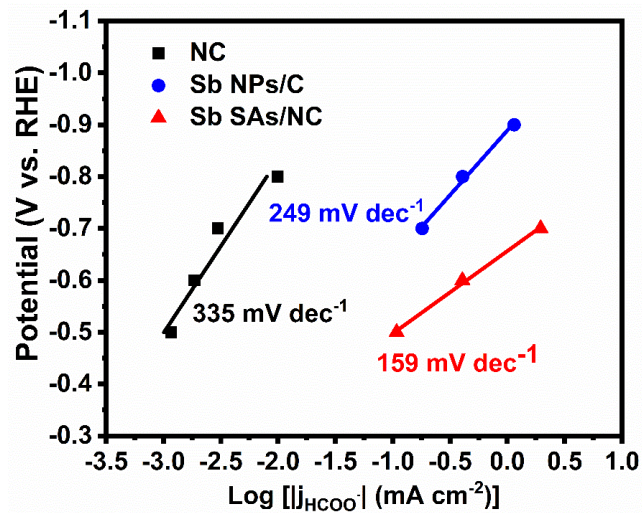


**Fig. S18.** Tafel plot of the partial HCOO<sup>-</sup> current density for Sb SAs/NC, Sb NPs/C and NC at different potentials.

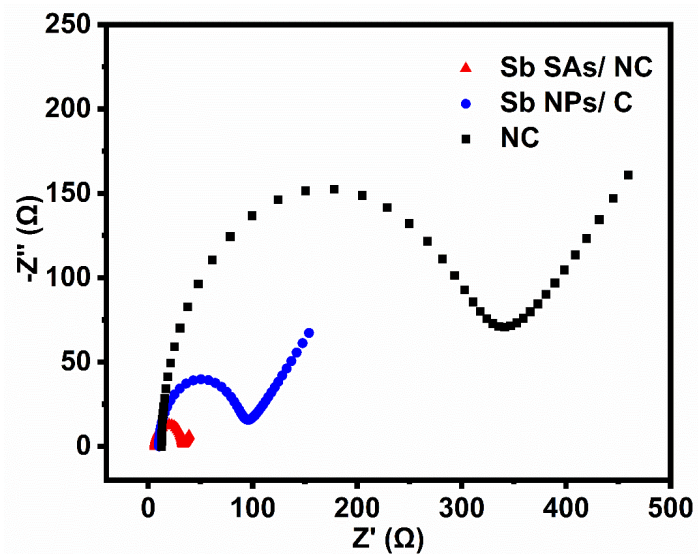


**Fig. S19.** Nyquist plots for Sb SAs/NC, Sb NPs/C and NC.

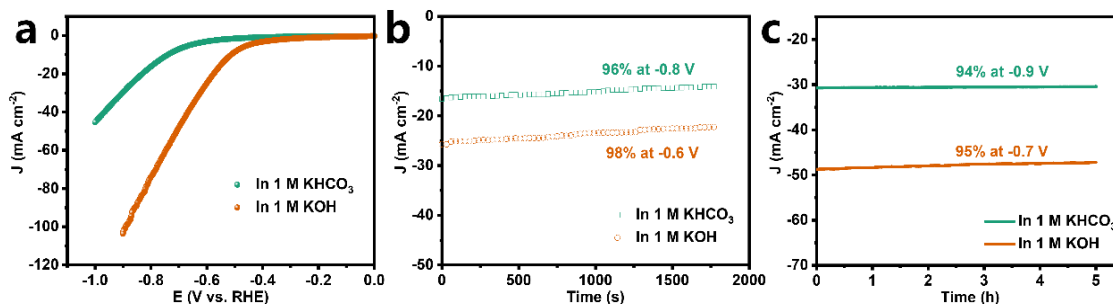


**Fig. S20.** (a) LSV curves, (b) Chronoamperometric responses at a few different potentials and (c) Long- term stability of Sb SAs/NC in 1 M KHCO<sub>3</sub> or 1 M KOH.

We deposited Sb SAs/NC on a gas diffusion layer and electrolyte is CO<sub>2</sub>-saturated 1 M KHCO<sub>3</sub> and 1 M KOH solution, respectively. We first tested the flow cell with 1M KHCO<sub>3</sub>. As shown in Fig. 20a (green line), the onset potential is about -0.6 V vs. RHE and lower than that value measured by H-type cell. Obviously, the current density has significantly increased due to rapid CO<sub>2</sub> diffusion, which is also a major advantage of using a flow cell. Rising FE formate indicated that the formate selectivity has also been improved (Fig. 20b). The use of alkaline electrolytes in flow cell for CO<sub>2</sub>RR process is another advantage. Therefore, we carried out the CO<sub>2</sub>RR experiments in flow cell in CO<sub>2</sub>-saturated 1 M KOH solution. The CO<sub>2</sub>RR onset potential was reduced to ~-0.44 V and the current density reached to 100 mA cm<sup>-2</sup> at -0.89 V in 1 M KOH. We also tested the stability of Sb SAs/NC (Fig. 20c) in flow cell. The current density and FE formate can keep in stable state for 5h. Thereafter, the electrolyte began to leak and the flow cell could no longer be used.

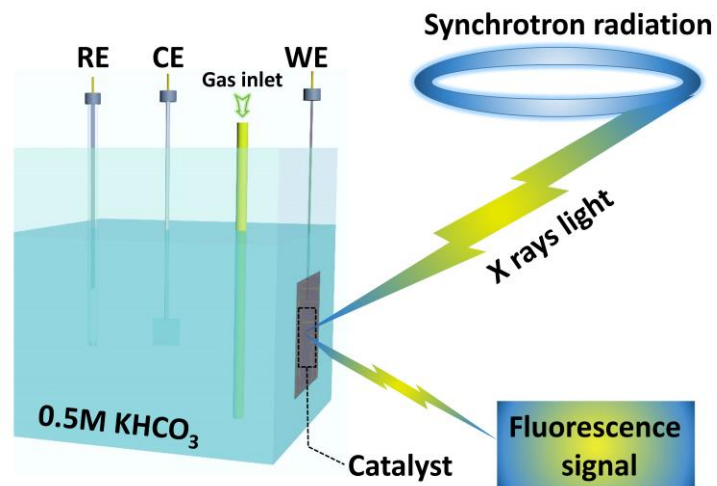


**Fig. S21.** Schematic model of electrochemical in situ cell setup. RE, reference electrode; CE, counter electrode; WE, working electrode.

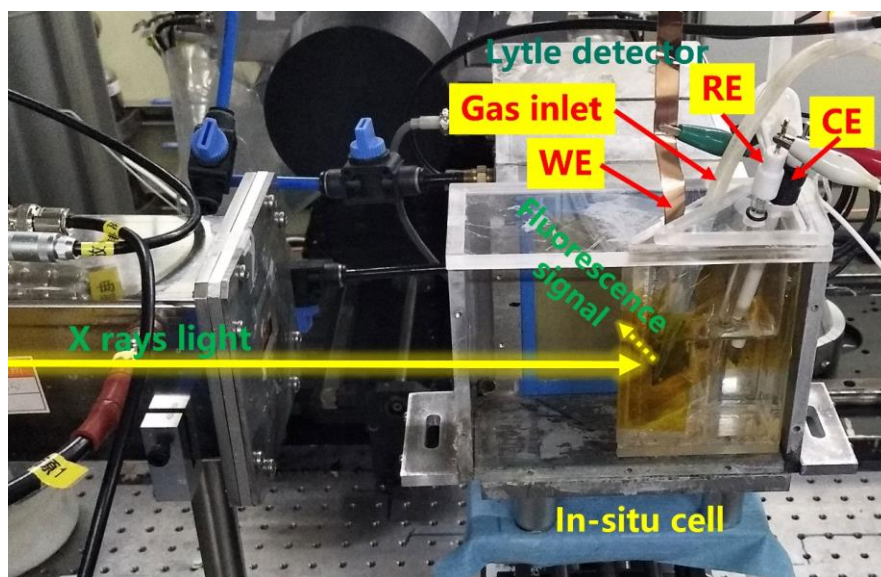


**Fig. S22.** The detail of the in-situ X-ray absorption spectroscopy measurement. The device is set up at 14W1 beam line with the support from SSRF, where the X-ray induced fluorescence model is applied.

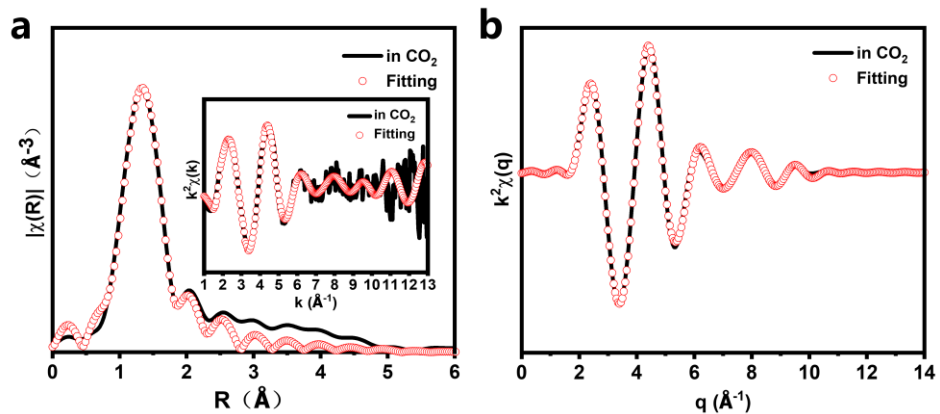


**Fig. S23.** (a) FT-EXAFS fitting curve (the inset is  $k$  space fitting curve) and (b) inversed FT-EXAFS fitting curve of the Sb SAs/NC immersing in  $\text{CO}_2$ -saturated 0.5 M  $\text{KHCO}_3$  without applied potential.

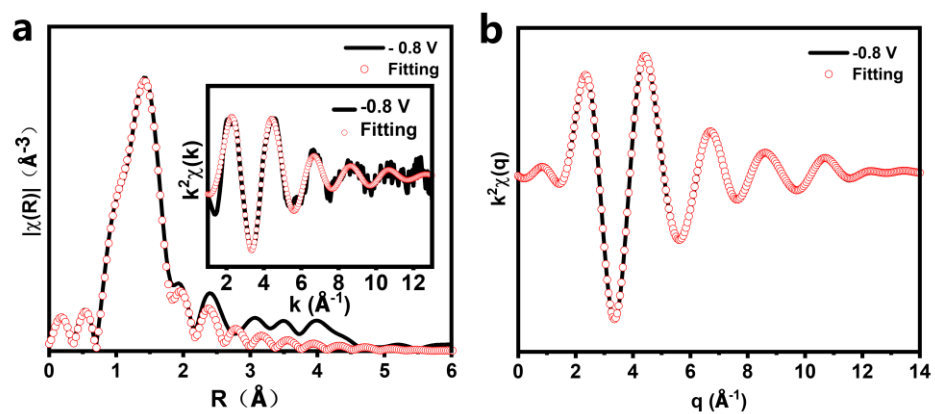


**Fig. S24.** (a) FT-EXAFS fitting curve (the inset is  $k$  space fitting curve) and (b) inversed FT-EXAFS fitting curve of the Sb SAs/NC at an applied potential of -0.8 V.

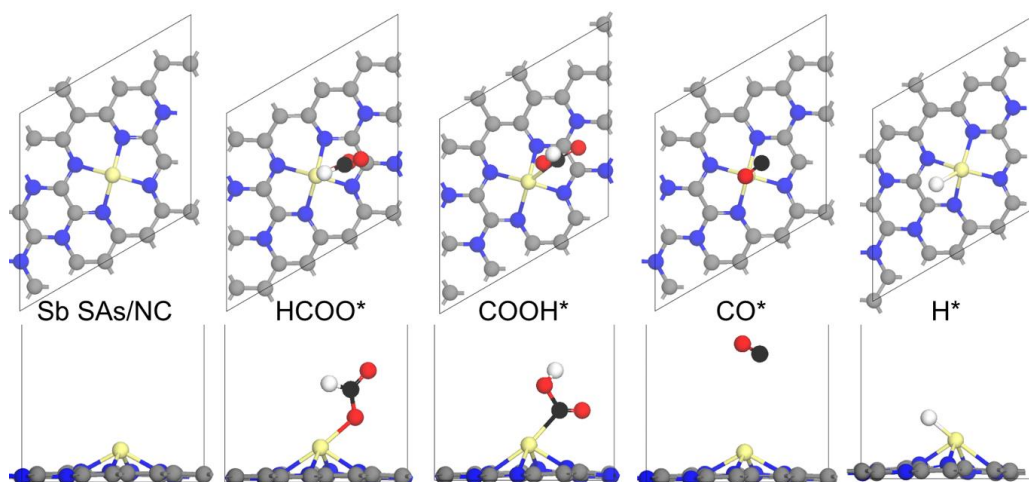


**Fig. S25.** Adsorption configurations of  $\text{HCOO}^*$ ,  $\text{COOH}^*$ ,  $\text{CO}^*$  and  $\text{H}^*$  on Sb SAs/NC (Yellow for Sb, gray for C in NC, blue for N, white for H, red for O, and black for C in reaction intermediates).

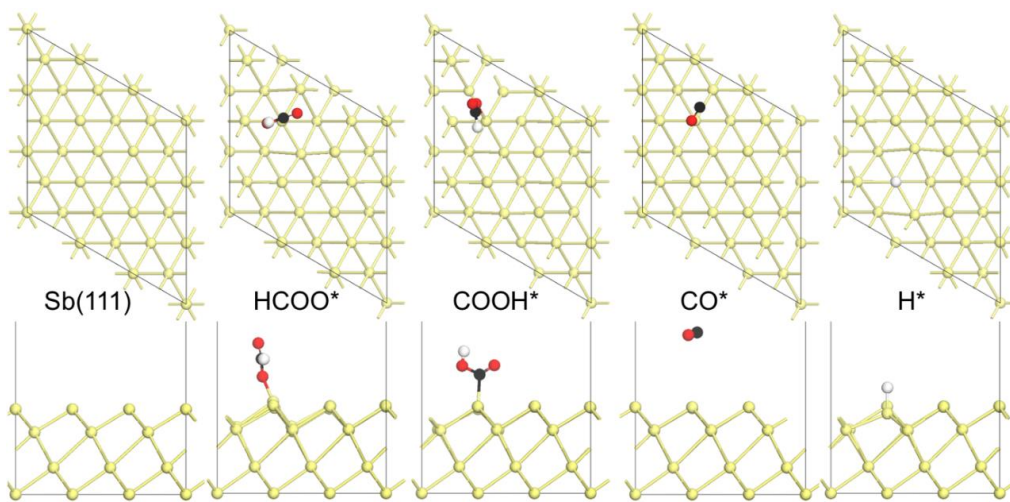


**Fig. S26.** Adsorption configurations of  $\text{HCOO}^*$ ,  $\text{COOH}^*$ ,  $\text{CO}^*$  and  $\text{H}^*$  on Sb(111) surface (Yellow for Sb, gray for C in NC, blue for N, white for H, red for O, and black for C in reaction intermediates).

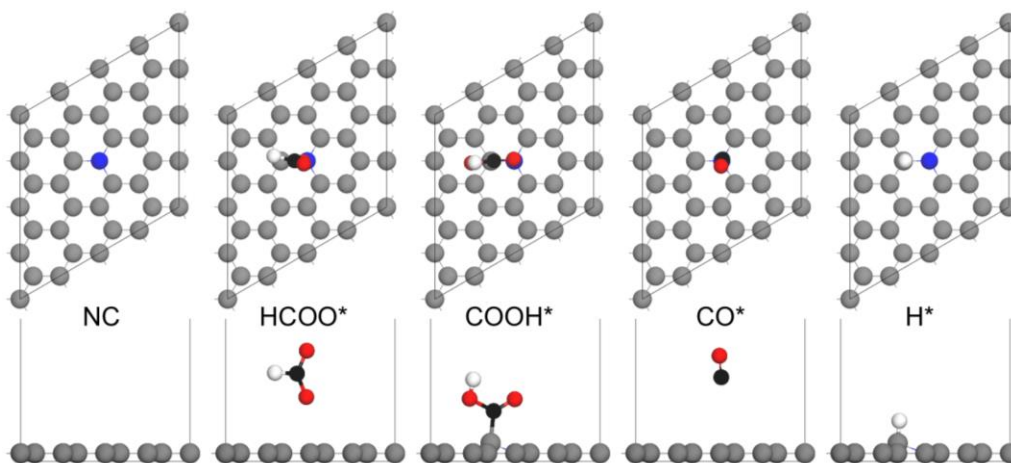


**Fig. S27.** Adsorption configurations of HCOO\*, COOH\*, CO\* and H\* on NC (gray for C in NC, blue for N, white for H, red for O, and black for C in reaction intermediates).

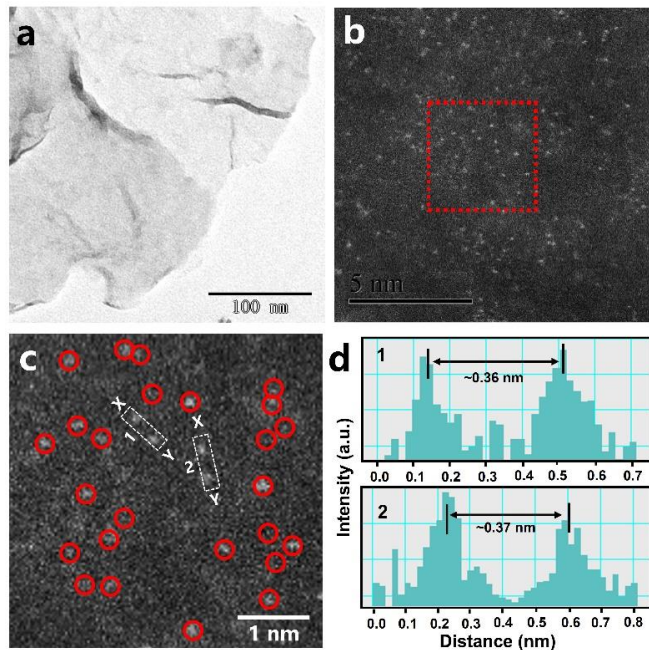


**Fig. S28.** (a) TEM image and (b, c) magnified HAADF-STEM images of In SAs/NC. (d) The corresponding intensity profiles along the line X-Y in c.

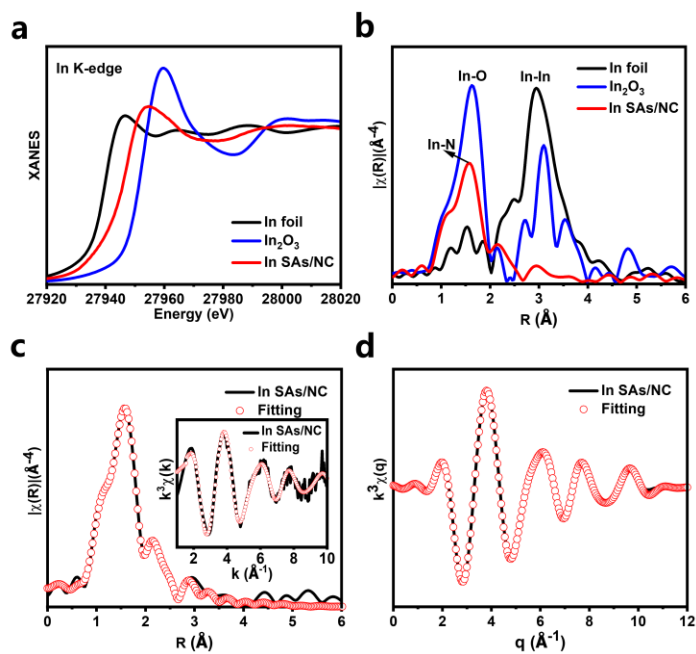


**Fig. S29.** (a) The XANES spectra and (b) The FT  $k^3$ -weighted In K-edge EXAFS spectra of In SAs/NC and references; (c) and (d) EXAFS fitting curves of In SAs/NC at In K-edge.

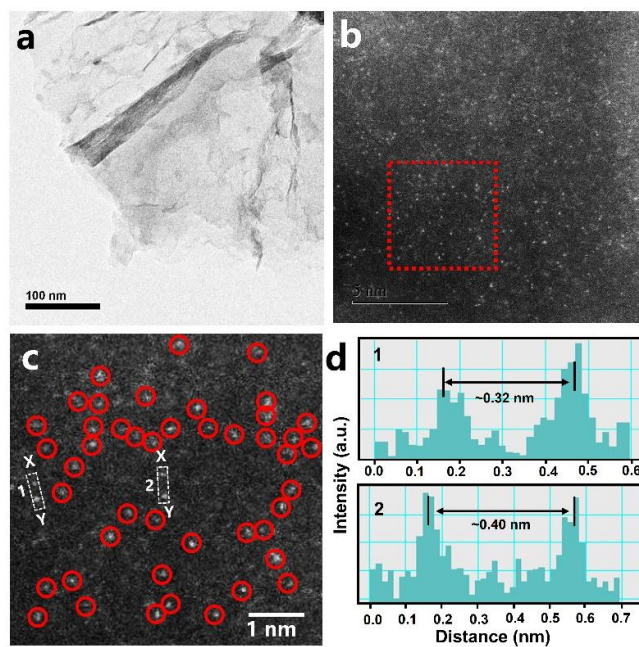


**Fig. S30.** (a) TEM image and (b, c) magnified HAADF-STEM images of Sn SAs/NC. (d) The corresponding intensity profiles along the line X-Y in c.

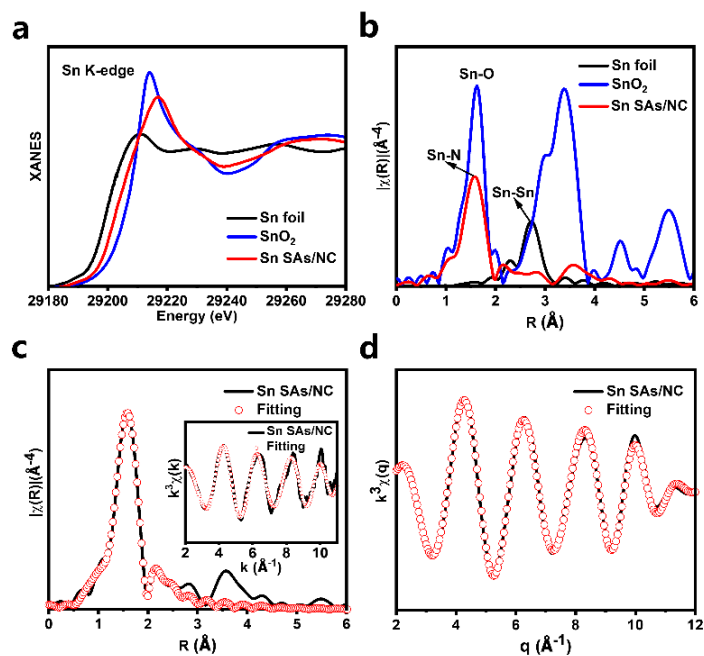


**Fig. S31.** (a) The XANES spectra and (b) The FT  $k^3$ -weighted Sn K-edge EXAFS spectra of Sn SAs/NC and references; (c) and (d) EXAFS fitting curves of Sn SAs/NC at Sn K-edge.

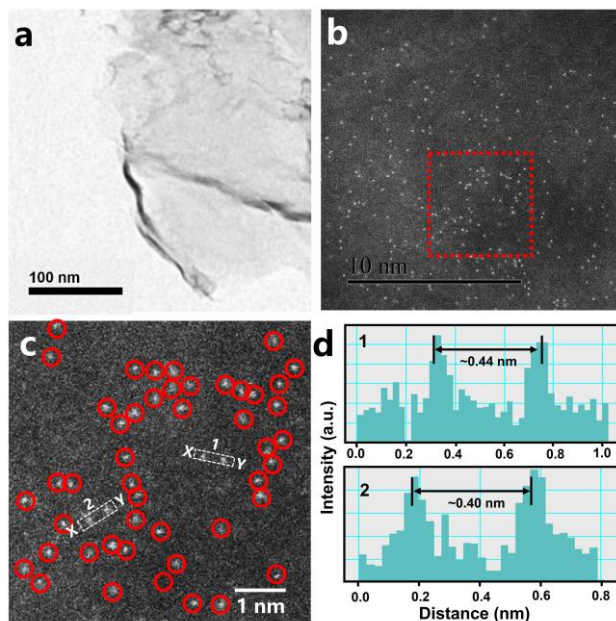


**Fig. S32.** (a) TEM image and (b, c) magnified HAADF-STEM images of Bi SAs/NC. (d) The corresponding intensity profiles along the line X-Y in c.

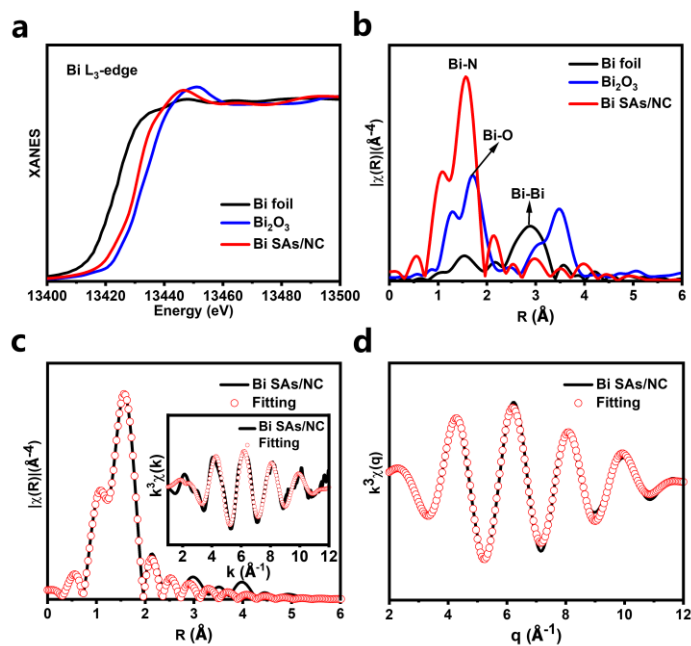


**Fig. S33.** (a) The XANES spectra and (b) The FT  $k^3$ -weighted Bi  $L_3$ -edge EXAFS spectra of Bi SAs/NC and references; (c) and (d) EXAFS fitting curves of Bi SAs/NC at Bi  $L_3$ -edge.

**Table S1. Structural parameters extracted from the Sb K-edge EXAFS fitting. ( $S_0^2=0.86$ )**

<i>sample</i>	<i>Scattering pair</i>	<i>CN</i>	<i>R</i> (Å)	$\sigma^2(10^{-3}\text{Å}^2)$	$\Delta E_0(\text{eV})$	<i>R factor</i>
Sb SAs/NC	Sb-N	$4.1 \pm 0.4$	$1.98 \pm 0.01$	$6.2 \pm 0.4$	$2.0 \pm 0.4$	0.004
Sb foil	Sb-Sb	12*	$2.69 \pm 0.01$	$5.8 \pm 0.5$	$2.0 \pm 0.6$	0.005

$S_0^2$  is the amplitude reduction factor; CN is the coordination number; R is interatomic distance (the bond length between central atoms and surrounding coordination atoms);  $\sigma^2$  is Debye-Waller factor (a measure of thermal and static disorder in absorber-scatterer distances);  $\Delta E_0$  is edge-energy shift (the difference between the zero kinetic energy value of the sample and that of the theoretical model). R factor is used to value the goodness of the fitting.

\* This value was fixed during EXAFS fitting, based on the known structure of Sb foil.

Error bounds that characterize the structural parameters obtained by EXAFS spectroscopy were estimated as  $N \pm 20\%$ ;  $R \pm 1\%$ ;  $\sigma^2 \pm 20\%$ ;  $\Delta E_0 \pm 20\%$ .

**Table S2. Comparison of CO<sub>2</sub>RR performance between Sb SAs/NC and other main group metal catalysts reported in the literatures under CO<sub>2</sub>-saturated electrolyte.**

<i>Catalyst</i>	<i>Electrolyte</i>	<i>Potential (V vs. RHE)</i>	<i>FE<sub>HCOO<sup>-</sup></sub>(%)</i>	<i>Reference</i>
<b>Sb SAs/NC</b>	<b>0.5 M KHCO<sub>3</sub></b>	<b>-0.8</b>	<b>94</b>	<b>This work</b>
SbNSs	0.5 M NaHCO <sub>3</sub>	-1.06	84	9
SnO <sub>2</sub> QWs	0.1 M KHCO <sub>3</sub>	-1.156	87.3	10
Bi <sub>2</sub> O <sub>3</sub> NSs	0.1 M KHCO <sub>3</sub>	-1.256	93.8	11
Sn-pNWs	0.1 M NaHCO <sub>3</sub>	-0.8	80	12
H-InO <sub>x</sub> NRs	0.5 M NaHCO <sub>3</sub>	-0.7	91.7	13
Mn-doped In <sub>2</sub> S <sub>3</sub> NSs	0.1 M KHCO <sub>3</sub>	-0.9	86	14
S <sub>2</sub> -In catalyst	0.5 M KHCO <sub>3</sub>	-0.98	93	15

**Table S3. Structural parameters extracted from the Sb K-edge EXAFS fitting of Sb SAs/NC in CO<sub>2</sub>-saturated 0.5 M KHCO<sub>3</sub> and at -0.8 V vs. RHE. ( $S_0^2=0.86$ )**

<i>sample</i>	<i>Scattering pair</i>	<i>CN</i>	<i>R</i> (Å)	$\sigma^2(10^{-3}\text{Å}^2)$	$\Delta E_0(\text{eV})$	<i>R factor</i>
Sb SAs/NC in CO <sub>2</sub>	Sb-N	4.1 ± 0.5	1.99 ± 0.01	5.7 ± 0.4	2.0 ± 0.4	0.005
	Sb-O	1.2 ± 0.5	2.00 ± 0.01	5.9 ± 0.6	0.4	
Sb SAs/NC at -0.8 V vs. RHE	Sb-N	4.0 ± 0.6	2.07 ± 0.01	5.9 ± 0.6	2.0 ± 0.5	0.005
	Sb-O	1.1 ± 0.5	2.01 ± 0.01	6.1 ± 0.5	0.5	

$S_0^2$  is the amplitude reduction factor; CN is the coordination number; R is interatomic distance (the bond length between central atoms and surrounding coordination atoms);  $\sigma^2$  is Debye-Waller factor (a measure of thermal and static disorder in absorber-scatterer distances);  $\Delta E_0$  is edge-energy shift (the difference between the zero kinetic energy value of the sample and that of the theoretical model). R factor is used to value the goodness of the fitting.

Error bounds that characterize the structural parameters obtained by EXAFS spectroscopy were estimated as  $N \pm 20\%$ ;  $R \pm 1\%$ ;  $\sigma^2 \pm 20\%$ ;  $\Delta E_0 \pm 20\%$ .

**Table S4. Structural parameters extracted from the In K-edge, Sn K-edge and Bi L<sub>3</sub>-edge EXAFS fitting. ( $S_0^2=0.86$ )**

<i>sample</i>	<i>Scattering pair</i>	<i>CN</i>	<i>R(Å)</i>	$\sigma^2(10^{-3}\text{Å}^2)$	$\Delta E_0(\text{eV})$	<i>R factor</i>
In SAs/NC	In-N	$4.0 \pm 0.7$	$2.01 \pm 0.01$	$7.0 \pm 0.5$	$1.5 \pm 0.5$	0.007
Sn SAs/NC	Sn-N	$4.2 \pm 0.5$	$1.90 \pm 0.01$	$5.8 \pm 0.4$	$1.5 \pm 0.4$	0.004
Bi SAs/NC	Bi-N	$3.9 \pm 0.5$	$1.99 \pm 0.01$	$6.3 \pm 0.6$	$1.5 \pm 0.4$	0.005

$S_0^2$  is the amplitude reduction factor; CN is the coordination number; R is interatomic distance (the bond length between central atoms and surrounding coordination atoms);  $\sigma^2$  is Debye-Waller factor (a measure of thermal and static disorder in absorber-scatterer distances);  $\Delta E_0$  is edge-energy shift (the difference between the zero kinetic energy value of the sample and that of the theoretical model). R factor is used to value the goodness of the fitting.

Error bounds that characterize the structural parameters obtained by EXAFS spectroscopy were estimated as  $N \pm 20\%$ ;  $R \pm 1\%$ ;  $\sigma^2 \pm 20\%$ ;  $\Delta E_0 \pm 20\%$ .

### 3. References

- 1 G. Kresse and J. Furthmüller, *Comput. Mater. Sci.*, 1996, **6**, 15–50.
- 2 G. Kresse and J. Furthmüller, *Phys. Rev. B*, 1996, **54**, 11169–11186.
- 3 P. E. Bloechl, *Phys. Rev. B*, 1994, **50**, 17953–17979.
- 4 D. Joubert, *Phys. Rev. B*, 1999, **59**, 1758–1775.
- 5 B. Hammer, L. B. Hansen and J. K. Nørskov, *Phys. Rev. B*, 1999, **59**, 7413–7421.
- 6 J. K. Nørskov, J. Rossmeisl, A. Logadottir, L. Lindqvist, J. R. Kitchin, T. Bligaard and H. Jónsson, *J. Phys. Chem. B*, 2004, **108**, 17886–17892.
- 7 A. A. Peterson, F. Abild-Pedersen, F. Studt, J. Rossmeisl and J. K. Nørskov, *Energy Environ. Sci.*, 2010, **3**, 1311–1315.
- 8 R. Jiang, L. Li, T. Sheng, G. Hu, Y. Chen and L. Wang, *J. Am. Chem. Soc.*, 2018, **140**, 11594–11598.
- 9 F. Li, M. Xue, J. Li, X. Ma, L. Chen, X. Zhang, D. R. MacFarlane and J. Zhang, *Angew. Chemie Int. Ed.*, 2017, **56**, 14718–14722.
- 10 S. Liu, J. Xiao, X. F. Lu, J. Wang, X. Wang and X. W. (David) Lou, *Angew. Chemie Int. Ed.*, 2019, **58**, 8499–8503.
- 11 S. Liu, F. X. Lu, J. Xiao, X. Wang and X. W. (David) Lou, *Angew. Chemie Int. Ed.*, 2019, **58**, 13828–13833.
- 12 B. Kumar, V. Atla, J. P. Brian, S. Kumari, T. Q. Nguyen, M. Sunkara and J. M. Spurgeon, *Angew. Chemie Int. Ed.*, 2017, **56**, 3645–3649.
- 13 J. Zhang, R. Yin, Q. Shao, T. Zhu and X. Huang, *Angew. Chemie Int. Ed.*, 2019, **58**, 5609–5613.
- 14 A. Zhang, Y. Liang, H. Li, X. Zhao, Y. Chen, B. Zhang, W. Zhu and J. Zeng, *Nano Lett.*, 2019, **19**, 6547–6553.
- 15 W. Ma, S. Xie, X. G. Zhang, F. Sun, J. Kang, Z. Jiang, Q. Zhang, D. Y. Wu and Y. Wang, *Nat. Commun.*, 2019, **10**, 892.